JOURNAL OF SPACECRAFT AND ROCKETS
Vol. 45, No. 4, July–August 2008

Optimal Design of Hypersonic Turbojet Engines for Two-Stage-to-Orbit Spaceplane

Hiroaki Kobayshi* and Hirokazu Suzuki†
Japan Aerospace Exploration Agency, Chofu, Tokyo 182-8522, Japan

DOI: 10.2514/1.31987

The Japan Aerospace Exploration Agency has been developing hypersonic (Mach 5+) turbojet engine technologies that are applicable to future two-stage-to-orbit spaceplanes and hypersonic transports. Experimental studies using a 1:10 scale model engine were conducted to acquire data for designing a full-scale practical engine in the next development phase. These experimental data improve the accuracy of an engine performance-prediction tool used at the Japan Aerospace Exploration Agency. This paper presents the most promising engine configuration derived using a multidisciplinary-design-optimization system that includes the newest performance-prediction tool for hypersonic turbojet engines. Quantitative comparison of turbine configurations, thermal protection methods, and fuel types showed that the engine most promising for minimizing the gross takeoff weight of a two-stage-to-orbit spaceplane is a hydrogen-fueled single-spool augmented turbojet with an airflow bypass.

Nomenclature

A_I	=	air inlet frontal area, m^2
A_P	=	air-precooler heat-exchange area, m^2
C_D	=	drag coefficient
C_L	=	lift coefficient
Cp_c	=	coolant specific heat capacity, J/kg/K
Cp_h	=	hot gas specific heat capacity, J/kg/K
D_A	=	ram-combustor diameter, m
D_B	=	combustion chamber diameter, m
D_C	=	compressor tip diameter, m
D_{IR}	=	air inlet diameter (ramjet mode), m
D_{IT}	=	air inlet diameter (turbojet mode), m
D_N	=	nozzle diameter, m
D_T	=	turbine tip diameter, m
d	=	heat-exchange-tube diameter, m
ER	=	equivalence ratio
ER_t	=	target equivalence ratio
g_c	=	critical pressure ratio (=0.53)
h	=	heat transfer coefficient, W/m^2/K
h_f	=	flight altitude, km
I_{sp}	=	specific impulse, s
L_v	=	vehicle length, m
M_f	=	flight Mach number
m_a	=	compressor flow rate, kg/s
m_c	=	coolant flow rate, kg/s
m_{fp}	=	modifying factor for air-breathing engine weight
m_{fs}	=	modifying factor for body structural weight
m_h	=	hot gas flow rate, kg/s
m_i	=	air inlet flow rate, kg/s
NTU	=	number of transfer units
N_e	=	number of rocket engines for second-stage orbiter
n_c	=	number of compressor stages
n_s	=	number of shafts
n_t	=	number of turbine stages
Pr	=	Prandtl number
P_c	=	combustion chamber pressure, MPa
P_i	=	fuel injection pressure, MPa
Q_c	=	compressor input power, kW
Q_t	=	turbine output power, kW
R	=	water equivalence ratio
Re	=	Reynolds number
S_{ref}	=	reference wing area, m^2
TIT	=	turbine inlet temperature, K
T_c	=	compressor exit temperature, K
$T_{c\max}$	=	limit compressor exit temperature, K
T_f	=	coolant exit temperature, K
$T_{f\max}$	=	limit coolant temperature, K
T_R	=	combustion temperature in the ram combustor, K
$T_{R\max}$	=	limit combustion temperature, K
$TIT_{\max}$	=	limit turbine inlet temperature, K
U_c	=	rotational speed of compressor, m/s
$U_{c\max}$	=	limit rotational speed of compressor, m/s
U_t	=	rotational speed of turbine, m/s
$U_{t\max}$	=	limit rotational speed of turbine, m/s
V_{mc}	=	mode-change speed (from turbojet to ramjet)
V_{sp}	=	second-stage separation speed
W_A	=	ram combustor weight, kg
W_B	=	combustion chamber weight, kg
W_C	=	compressor weight, kg
W_{eng}	=	total weight of air-breathing engine, Mg
W_{fuel}	=	propellant weight of first-stage vehicle, Mg
W_{fuel2}	=	propellant weight of second-stage orbiter, Mg
W_{gtot}	=	total vehicle gross weight, Mg
W_I	=	air inlet weight, kg
W_N	=	nozzle weight, kg
W_P	=	air precooler weight, kg
W_{str}	=	body structural weight of first-stage vehicle, Mg
W_{sub}	=	subsystems weight of first-stage vehicle, Mg
W_T	=	turbine weight, kg
W_{tnk}	=	propellant tank weight of first-stage vehicle, Mg
W_2	=	total weight of second-stage orbiter, Mg
α	=	angle of attack, rad
η_h	=	temperature efficiency
λ	=	thermal conductivity, W/m/K

Presented as Paper 8051 at the 14th AIAA/AHI Space Planes and Hypersonic Systems and Technologies Conference, Canberra, Australia, 6–9 November 2006; received 6 May 2007; revision received 27 February 2008; accepted for publication 27 March 2008.

*Researcher, Jet Engine Technology Research Center, 7-44-1 Jindaiji-higashi. Member AIAA.
†Senior Researcher, Future Space Transportation Research Center, 7-44-1 Jindaiji-higashi. Member AIAA.

I. Introduction

HYPERSONIC turbojet engines are promising propulsion systems for future space transportation. Although it is difficult to use current aircraft gas turbine engines at speeds above Mach 3, engines whose turbo machinery is protected from excessive heat

hypersonic flight can be used at speeds greater than Mach 5. Flow diagrams of hypersonic turbojet engines that have been studied in the United States, Europe, and Japan are shown in Fig. 1.

A precooled turbojet (PCTJ) engine has a heat exchanger to cool air upstream of the compressor using low-temperature fuel (e.g., liquid hydrogen or liquid methane). A single-coolant system or dual-coolant system can be selected for this engine. A single-coolant system uses the cryogenic fuel to cool the air directly, and a dual-coolant system uses primary (fuel/helium) and secondary (helium/air) heat exchangers. The dual-coolant system is more complicated but safer. As an alternative means of being equipped with a heat exchanger, some PCTJ engines inject water or liquid oxygen directly in front of the compressor. In the United States, conceptual studies of PCTJ engines were reported in 1988 by Powell and Glickstein (Pratt & Whitney, Inc.) [1]. In Japan, development of the 1000-kN class subscale PCTJ engine (the *S* engine) was started in 2004 after analytical studies by Taguchi et al. at the National Aerospace Laboratories [2]. In the United Kingdom, an air-precooled turbo-rocket engine called the Sabre engine is being developed at Reaction Engines, Ltd. [3].

A turboramjet (TRJ) engine captures all the hot air upstream of the compressor and leads it, via a bypass duct, into the combustor downstream of the turbine to protect the turbo machinery during hypersonic flight. A variable geometry vane is used to control air flow rate through a bypass duct enveloping the whole core turbojet. The TRJ engine is an extended concept of the variable-cycle engines used for current supersonic aircraft. In Japan, the Engineering Research Association for Super/Hypersonic Transportation Project System has been developing the Mach 5+ TRJ engine (HYPR program) since 1989. This engine was tested successfully at General Electric's Altitude Test Facility [4].

An air turboramjet (ATR) engine drives a turbine with highly pressurized gas that is independent of the main airflow passing through the compressor, thereby avoiding imposition of a severe constraint on the turbine inlet temperature during high-speed flight. An expander cycle or a gas-generator cycle can be selected as a design option. The former drives a turbine with fuel that is vaporized in a heat exchanger, whereas the latter uses combustion gas supplied from a small gas generator. The feasibility of the liquid-hydrogen-fueled expander cycle ATR engine was confirmed both in the United States with the model 304 demonstration engine (Pratt & Whitney, Inc.) [5] and in Japan with the air turboramjet engine with expander cycle (ATREX) engine developed at the Institute for Space and Aeronautical Science (ISAS) [6]. A photograph of the ATREX engine firing under sea-level static conditions is shown in Fig. 2. The gas-generator ATR is also under development at the Japan Defense Agency [7].

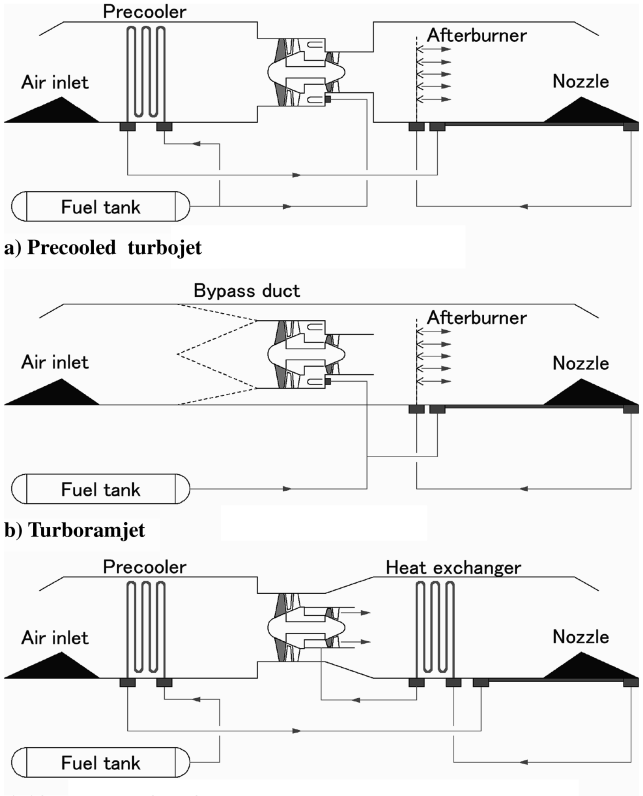

Fig. 1 Flow diagrams of representative hypersonic turbojet engines.

II. Performance-Prediction Tool for Hypersonic Turbojet Engines

The propulsive performance of hypersonic turbojet engines can be estimated using a performance-prediction tool that was developed at the Japan Aerospace Exploration Agency (JAXA) and has three modules: 1) a general-purpose turbofan engine simulator, 2) an engine weight analysis tool, and 3) a thermo-physical properties database. Several design options can be attached for hypersonic flight. This tool is useful not only as a stand-alone application for estimating engine thrust, specific impulse, and engine weight but also, as shown in Fig. 3, as a subroutine that can be called by the Systems Evaluation and Analysis Tool (SEAT), which is JAXA's integrated design environment for reusable space transportation systems, including the air-breathing two-stage-to-orbit (TSTO). Each module in the hypersonic turbojet engine performance-prediction tool is described as follows.

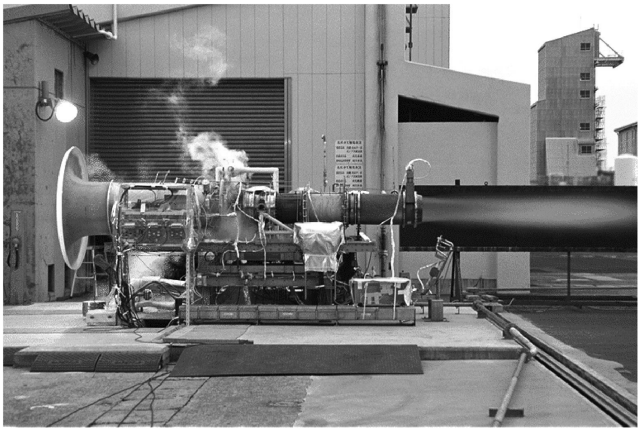

Fig. 2 Combustion test of the ATREX-500 engine at the Noshiro Testing Center [6].

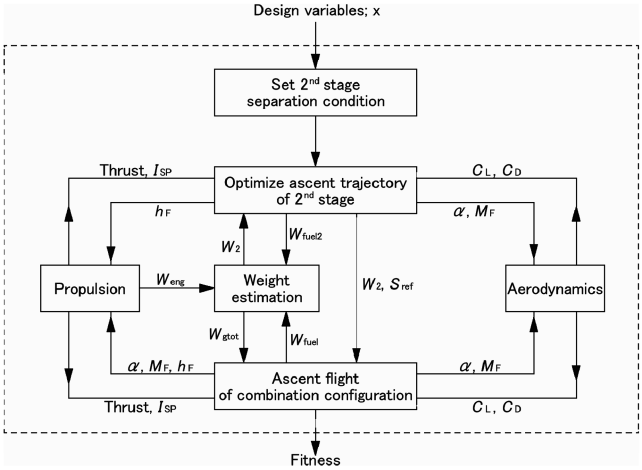

Fig. 3 Diagram of data flow in SEAT design of a TSTO spaceplane.

Table 1 Design point performance of the reference compressor and turbine

Corrected flow rate of the compressor	177.0 kg/s
Compressor pressure ratio	6.2
Compressor efficiency	0.854
Compressor tip speed	550.0 m/s
Turbine adiabatic efficiency	0.878
Turbine tip speed	480.0 m/s

A. Turbofan Engine Simulator

A multispool turbofan was the core engine of the hypersonic turbojet in the work reported here, and important items in designing a core engine are the number of compressor stages, the number of turbine stages, the number of shafts (single spool or multispool), compressor diameter, turbine diameter, and the turban inlet temperature. The bypass ratio and power distribution between the fan and compressor can also be changed. Maps of the four-stage axial flow compressor (diameter = 1.2 m) and the two-stage reaction turbine (diameter = 1.152 m), the characteristics of which were obtained during ATREX engine development at the ISAS, were often used as reference data in this study. Design point specifications are listed in Table 1.

The compressor map is properly expanded when it used as a map for a compressor with a different pressure ratio and a corrected airflow rate. The compressor stage pressure ratio is 1.4 on average, and the turbine efficiency (calculated from the turbine output power per stage) is shown in Fig. 4 as a function of the speed ratio (rotational speed divided by the isentropic exhaust speed). If a weight increase penalty is permitted, turbine efficiency can be increased by increasing the number or diameter of turbine stages because doing so increases the speed ratio. Because of the lower heating value of fuel-air combustion, the combustion efficiency of the ATREX engine is usually 90% that of the minimum value guaranteed for a hydrogen combustor with a simple fuel injection system. The inlet pressure is usually reduced by 4% because of combustion pressure loss.

In this module of the performance-prediction tool, the operations of air systems are simulated serially from the compressor inlet to the turbine outlet, and fuel systems are simulated serially from the boost pump inlet to the injector outlet. The five unknown values listed in Table 2 must be determined to form a turbofan engine cycle. The multidimensional Newton–Raphson method is used to satisfy the five constraints listed in Table 3. Even though constraints F_2 and F_4 are max functions with discontinuous differential, they do not reduce the converging speed.

F_1, which is mainly used to decide the value of X_1, requires the power of the turbine to be equal to that of the compressor. F_2 actually comprises four constraints: one for airflow matching between the air inlet and compressor and three for the maximum compressor exit air temperature and the maximum mechanical and corrected rotational speeds of the compressor. The compressor airflow rate should be increased even if all constraints in F_2 are satisfied. In supersonic flight, air that cannot be taken in to the compressor is bled outside without generating thrust. Therefore, compressor and air inlet sizes should be optimized. Increasing the air inlet size is an effective way to gain a thrust margin at Mach 5 or 6. On the other hand, a larger air inlet results in a lower thrust-to-weight ratio and surplus air at Mach 2 or 3. The compressor should operate under partial loading to keep the outlet air temperature from increasing excessively when the number of stages or the engine inlet temperature is increased. To simplify the evaluation of the partial-load performance of the compressor, we restricted the operating points on the compressor map to a single line (constant surge margin X_3). The compressor-corrected airflow rate, pressure ratio, and efficiency are determined for a given rotational speed. F_{41}, which is used mainly to decide the value of X_4, is the upper limit of TIT. Because any value of X_4 can be selected when F_{41} is inactive, F_{42} is introduced as an additional constraint. In this study, the target equivalence ratio is one design variable that is optimized. The choking condition X_5 is imposed at the fuel injector to determine the boost pump outlet pressure. A boost pump driven by some of the turbine shaft power is used to supply fuel against friction loss and choking pressure. The boost pump design was not considered in this study because the boost pump power is only 2–3% of the turbine shaft power.

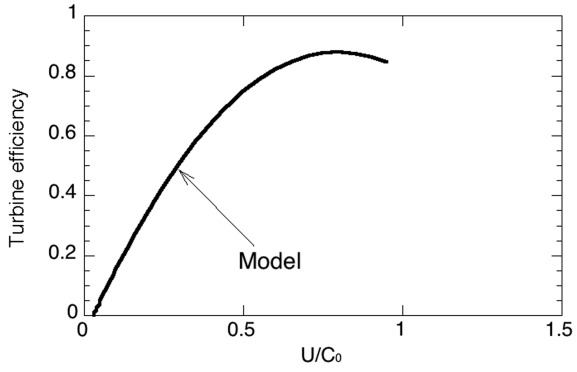

Fig. 4 Turbine efficiency versus speed ratio for the model used in this study.

Table 2 Unknown variables

X_1	Turbine pressure ratio
X_2	Compressor flow rate
X_3	Compressor surge margin
X_4	Fuel flow rate
X_5	Fuel pump pressure

Table 3 Constraints

F_1	$F_1 = Q_t - Q_c = 0$
F_2	$F_2 = \max(F_{21}, F_{22}, F_{23}, F_{24}) = 0$
	$F_{21} = m_a - m_i$
	$F_{22} = U_c - U_{c\max}$
	$F_{23} = U_t - U_{t\max}$
	$F_{24} = T_c - T_{c\max}$
F_3	$F_3 = X_3 = \text{constant}$
F_4	$F_4 = \max(F_{41}, F_{42}) = 0$
	$F_{41} = TIT - TIT_{\max}$
	$F_{42} = ER - ER_t$ ($ER_t < 1.0$, lean burn)
	$F_{42} = ER_t - ER$ ($ER_t < 1.0$, rich burn)
F_5	$F_5 = P_i - P_c/g_c$

Data for the air inlet performance model was obtained in wind-tunnel experiments with the Mach 5.3 mixed-compression supersonic inlet that were conducted at JAXA. The total-pressure-recovery and mass-capture-ratio data are shown in Fig. 5 as a function of flight speed in which one sees that the performances of the air inlet model in this conceptual study were slightly lower than the military specifications. The mass-capture ratio at subsonic speeds was estimated with the choking condition at the minimum flow path area in the air inlet. The airflow rate can be changed in agreement with the compressor's demand unless that demand exceeds the inlet maximum capture flow rate. The 4% of the captured air that is bled to reduce the thickness of the boundary layer generates no thrust. The nozzle efficiency is defined as the ratio of the actual gross thrust to the ideal gross thrust, which is the product of combustion gas flow rate and isentropic exhaust speed (assuming that combustion gas expands isentropically from its volume at the chamber pressure to its volume at the ambient pressure). The installed net thrust is derived by subtracting the ram drag and external friction drag from the gross thrust corresponding to the nozzle thrust efficiency. The nozzle thrust efficiency data (Fig. 6) was obtained in a three-dimensional computational fluid dynamics (CFD) analysis of a rectangular variable-area nozzle designed for the Mach 5+ hypersonic turbojet. The General Aerodynamic Simulation Program (Aerosoft, Inc.) was also used to calculate nozzle thrust efficiency at Mach numbers from 3 to 6. The engine simulator in the performance evaluation tool we used calculates external hypersonic airflow and internal air-hydrogen

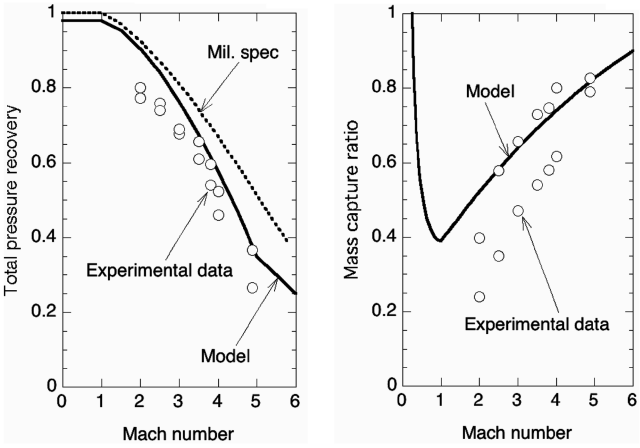

a) b)

Fig. 5 Inlet performance models: a) total-pressure recovery, b) mass-capture ratio.

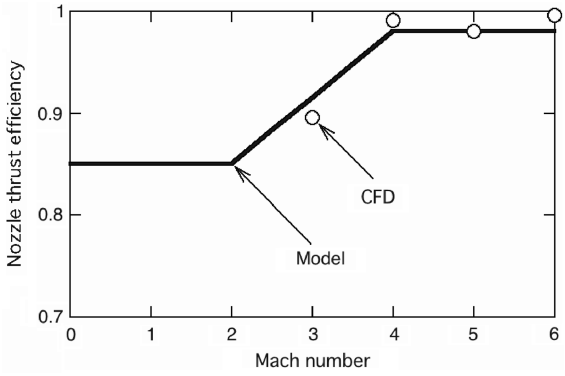

Fig. 6 Relation between nozzle thrust efficiency and Mach number that was used in this study.

combustion gas flow simultaneously, so the effect of nozzle boat tail drag is included in the nozzle thrust efficiency.

B. Engine Weight Analysis Tool

The engine weight analysis tool in this study is based on empirical expressions developed by Sagerser et al. for use in analysis of vertical takeoff and landing (VTOL) power plants [8]. The engine weight model for that study was obtained from a several documents related to characteristics of engines, and comparisons showed that estimated engine weights were within 10% of the actual weights. Some corrections and simplifications were added to suit our hypersonic engine analysis. As shown by the following expressions, the weight of engine components, including the compressor, combustor, and turbine, can be presented as functions of the number of stages and the reference length.

$$W_C = 103\min(n_C, 2)D_C^{2.7} + 24.7\max(0, n_C - 2)^{1.2}D_C^{2.2} \quad (1)$$

$$W_T = 312 n_T D_T^{2.5} \quad (2)$$

$$W_B = 78 D_B^2 \quad (3)$$

$$W_I = 203 A_I + 137 A_I^2 \quad (4)$$

$$W_N = 142 D_N^2 \quad (5)$$

The equation for air inlet weight W_I was derived from three-dimensional finite element method (FEM) analysis of the variable-geometry inlet designed for the Mach 5+ hypersonic turbojet. The engine weight analysis tool also adds 41 kg as the weight of accessories that are independent of engine scale. Additional weight, including that of bolt and nuts, tube and valves, and that needed for margins, is simply modeled as 17% of the total engine weight.

C. Thermo-Physical Properties Database

The International Standard Atmosphere (ISA) was referred to produce an atmospheric pressure and temperature model as a function of altitude. Thermal properties of air and combustion gas were presented as functions of pressure and temperature using enthalpy and entropy maps of constituent gases. This database includes a cryogenic liquid properties table summarized by NASA [9,10]. Sutherland's formula and improved Eucken's formula were used to estimate the viscosity and thermal conductivity.

III. Design Options for Hypersonic Flight

A. Fuel Type

Specific impulse can be increased by using liquid hydrogen or methane instead of the kerosene fuel used in current aircraft because those fuels have larger heating values per unit mass. The values listed in Table 4 show that liquid hydrogen and liquid methane are both better for cooling the regenerative combustion chamber and the air-precooling heat exchanger because their cooling capacities are greater than the cooling capacity of kerosene. On the other hand, densities of these cryogenic fuels are lower than that of kerosene, and this means that larger volumes of fuel tanks are required. Moreover, a tank filled with a cryogenic fuel, as well as the tubes and valves through which that fuel flows, must be covered with insulating materials to prevent excessive heating when the spaceplane is cruising at hypersonic speeds. A multidisciplinary-design-optimization (MDO) analysis can determine the best type of fuel for a TSTO spaceplane.

B. Variable Bypass Ratio

The bypass ratio is the amount of air passing through the bypass duct divided by the amount of air passing through the core engine. An engine with a higher bypass ratio has a lower specific thrust but a better specific fuel consumption (SFC), and vice versa. By varying the bypass ratio, the engine cycle can be modified to maintain good performance on a flight trajectory in a greatly changing environment. For example, maximum thrust is preferable during the ascent phase, and a better SFC is preferable during the cruising phase. As described previously, the TRJ engine bypasses all captured hot air upstream of the compressor when it is operating in the ramjet mode. This is an effective way to protect the core engine, which is unnecessary during hypersonic flight, from aerodynamic heating. The bypassed air flows through a duct surrounding the core engine and mixes with

Table 4 Tradeoff table used in selecting the fuel type

	Kerosene	Liquid methane	Liquid hydrogen
Heating value, MJ/kg	43 (Good)	50 (Better)	121 (Best)
Cooling capacity, kJ/kg	0 (No good)	−950 (Better)	−4430 (Best)
Density, kg/m^3	800 (Best)	424 (Better)	70.8 (No good)
Storability	(Best)	(Better)	(No good)
Environmental impact	(No good)	(No good)	(Best)

Cooling capacity: enthalpy drop from standard temperature (273.15 K) and pressure (0.1013 MPa)

Table 5 Additional unknown variable and constraint for the variable-bypass-ratio option

X_6	Rate of secondary fuel flow into the ram combustor
F_6	$F_6 = T_R - T_{R\max} = 0$

core-engine exhaust and secondary fuel in the ram combustor downstream of the turbine. The total pressure of the bypass air and that of the core-engine exhaust was set to the lower value to evaluate their mixing loss simply. Additional unknown variables and constraints for this option are listed in Table 5. A drawback of this option is the weight increase, which is shown as the following expression including the ram combustor, flow control valve, and bypass duct:

$$W_A = 387D_A^2 \tag{6}$$

C. Air Precooling

Installing an air precooler upstream of the compressor extends the flight envelope of the vehicle beyond Mach 4 by reducing the compressor exit air temperature. It also increases the thrust because less power is needed for compressing cooler and denser air. There are, however, three penalties that accompany air precooling. The first is the increased weight of the engine structure. The weight increase can be evaluated using the following expression, in which the precooler weight W_P is included the weight of the heat-exchange tubes and the manifolds, the weight of which is approximately 50% that of the tubes. The precooler being developed at JAXA contains several stainless steel tubes that are 2 mm in diameter and have walls 0.1 mm thick.

$$W_P = 1.128A_P \tag{7}$$

The second penalty of air precooling is an increase in total pressure loss due to frost formation on heat-exchange tubes when humid air enters the precooler. This frost also degrades the heat-exchange performance of the precooler. Air-precooling operations should therefore be started at altitudes above 10 km. The third penalty is the decreasing surge margin and airflow pumping capability of the compressor attributable to inlet temperature distortion.

If the air precooler is a fully counterflow type, which has the best heat-exchange performance among shell-type and tube-type heat exchangers, its temperature efficiency is determined by the number of transfer units (NTU) and the water equivalence ratio R. The temperature efficiency η_h was estimated using Zukauskas's formula. The effect of coolant-wall heat transfer and heat conductivity in the wall is not included in Zukauskas's formula because these are negligible relative to the air-wall heat transfer. A correlation factor c was introduced to express the performance deterioration resulting from frost formation and other factors. Values of the temperature efficiency determined experimentally acquired using the 200-kW-class LH2-air precooler developed for the S engine are plotted against R in Fig. 7, which also shows the efficiency vs R curves calculated for an ideal counterflow heat exchanger and the heat-exchanger model used in the present work. The appropriate value of c was determined to be 0.9. The air pressure drop was obtained by multiplying the friction loss coefficient C_f and dynamic pressure calculated from the mean airflow speed between heat-exchange tubes. The value of C_f acquired in experiments with dry air was approximately 10. To account for the effects of frost formation, we used a C_f of 35. Additional unknown variables and constraints for this option are listed in Table 6. The compressor exit air temperature is thus determined not by the rotational speed of the turbine but by the rate at which coolant flows through the precooler.

$$\eta_h \equiv \frac{T_{h,\text{out}} - T_{h,\text{in}}}{T_{h,\text{in}} - T_{c,\text{in}}} = \frac{1 - \exp[-(NTU)(1-R)]}{1 - R\exp[-(NTU)(1-R)]} \tag{8}$$

$$NTU = \frac{hA_P}{m_h Cp_h} \tag{9}$$

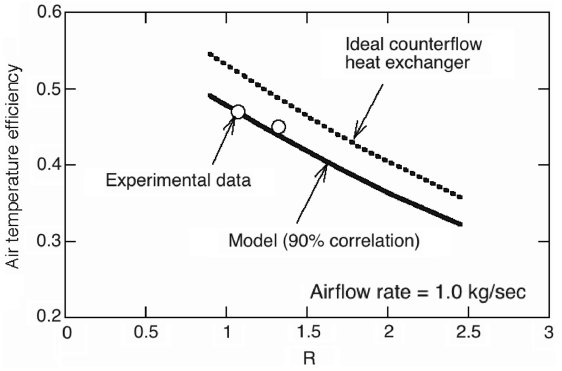

Fig. 7 Temperature efficiency of the air precooler.

$$R = \frac{m_h Cp_h}{m_c Cp_c} \tag{10}$$

$$h = \frac{\lambda}{d} 0.27 Re_d^{0.63} Pr^{0.36} \tag{11}$$

IV. Performance Characteristics of Hypersonic Turbojet Engines

This section describes the predicted performance of hypersonic turbojet engines and quantitatively compares the effects of various turbine configurations, thermal protection methods, and fuel types. Propulsive constraints commonly imposed in this study are listed in Table 7. Engine performances on the representative trajectory of the air-breathing TSTO (dynamic pressure = 50 kPa) are evaluated for Mach numbers from 0 to 7.

The specific impulse I_{sp} of an augmented turbojet engine is shown as a function of Mach number in Fig. 8 for engines with various numbers of compressor stages. The I_{sp} improves monotonically with increasing stage number from 1 to 5. When the stage number is 6 or more, however, the I_{sp} decreases at higher flight speeds because partial operation is imposed to reduce air temperature at the exit of the compressor by reducing the rotational speed. Because the number of compressor stages optimal for low-speed flight differs from the number optimal for high-speed flight, a quantitative trade-off analysis should be conducted. Figure 9 shows that reheating increases the specific thrust of a turbojet engine with a five-stage compressor but decreases its I_{sp}.

Specific impulse characteristics of augmented turbojet engines with heat-protecting devices are plotted in Fig. 10. The specific impulse of the turbojet (TJ) engine decreases with Mach number and at Mach 2 is exceeded by that of the ramjet (RJ) engine. Consequently, the operation mode of the TRJ engine should be changed from TJ to RJ at Mach 2. Although reducing the target

Table 6 Additional constraint for air precooling

F_4	$F_4 = \max(F_{41}, F_{42}, F_{43}, F_{44}) = 0$
	$F_{41} = TIT - TIT_{\max}$
	$F_{42} = ER - ER_t$ ($ER_t < 1.0$, lean burn)
	$F_{42} = ER_t - ER$ ($ER_t > 1.0$, rich burn)
	$F_{43} = T_c - T_{c\max}$
	$F_{44} = T_f - T_{f\max}$

Table 7 Constraints on engine operation commonly imposed in this study

Maximum corrected rotational speed of the compressor	600 m/s
Maximum mechanical rotational speed of the compressor	550 m/s
Maximum turbine inlet temperature	1723 K
Maximum afterburning temperature	2773 K
Maximum compressor exit temperature	720 K

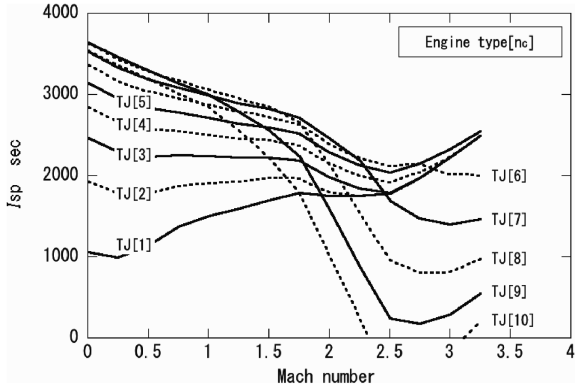

Fig. 8 Effect of the number of compressor stages on specific impulse.

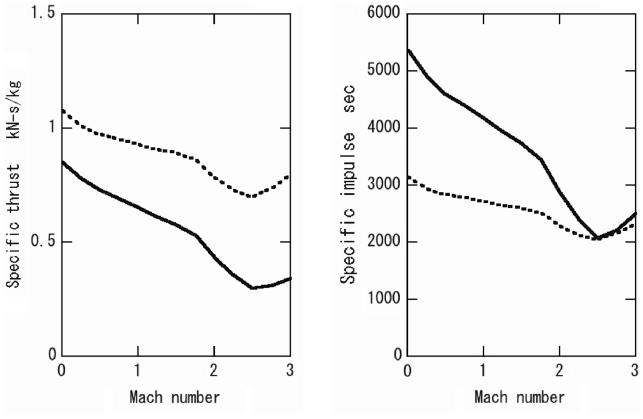

a) **b)**

Fig. 9 Thrust performance of a turbojet engine with 5-stage compressor with (dotted line) and without (solid line) reheating.

equivalence ratio improves the specific impulse in the RJ mode, the specific thrust (the thrust per unit airflow rate) still decreases. A secondary air inlet should therefore be installed to generate sufficient thrust. Air precooling, in contrast, improves the thrust performance and extends the operation envelope of the TJ engine to hypersonic speeds. Increasing the coolant flow rate reduces the compressor exit air temperature. Consequently, more compressor stages can be permitted for the PCTJ engine. At hypersonic velocities, however, the I_{sp} of the PCTJ engine is inferior to that of the RJ engine because the fuel equivalence ratio of the PCTJ engine must be increased to satisfy thermal constraints on the compressor exit temperature. The break-even point is located at approximately Mach 4. The hatched area in Fig. 10 shows the relative gains. Figure 11 shows that at any Mach number between 0 and 7 the specific impulse of a PCTJ engine burning liquid hydrogen is greater than that of a TJ engine burning kerosene, liquid methane, or liquid hydrogen.

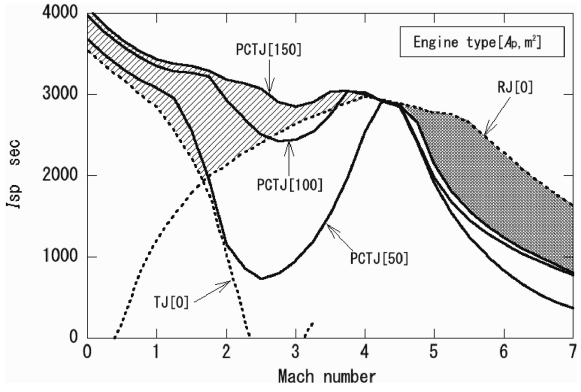

Fig. 10 Effect of heat protection devices on the specific impulse of a turbojet engine with a 10-stage compressor.

The thrust-to-weight ratio of a PCTJ engine is plotted in Fig. 12 against a representative length (air inlet diameter). Because engine weight is proportional to approximately the 2.5th power of a representative length, the engine thrust-to-weight ratio decreases with increasing engine size. The fraction of engine weight that is independent of engine scale, however, increases as engine size decreases. As a result, the thrust-to-weight ratio of a PCTJ is greatest when the compressor tip diameter is 0.5 m. The modifying factor for engine structural weight (m_{fp}) was set as 0.8. Engine weight reduction can be achieved by applying advanced carbon–carbon composite materials [11].

V. Multidisciplinary Design Optimization of a Two-Stage-to-Orbit Spaceplane

A. Problem Formulation

This chapter presents the results of a search for the engine system most promising for the fully reusable TSTO spaceplane using the present hypersonic turbojet engine technologies. The mission requirement is to carry a 1 ton payload to a low earth orbit. The TSTO system in this paper comprises a first-stage high-speed airplane that takes off and lands horizontally using air-breathing engines and a second-stage wing-body-shaped orbiter powered by LE-7-class rocket engines. The vehicle, which has a large delta wing, a body with a rectangular cross section, and a second stage on its back, is shown schematically in Fig. 13. It has two retractable canard wings in the nose to improve its takeoff and landing capabilities. The canard wings are retracted into the nose at speeds greater than Mach 1. Four air-breathing engines are installed on each side of the fuselage as shown in Fig. 14. The bottom surface of the fuselage might be a better location for a hypersonic engine because precompression of air upstream of the inlet improves the engine performance. An important disadvantage of that location, however, is that particles on the runway that are churned up by the front wheel are easily introduced

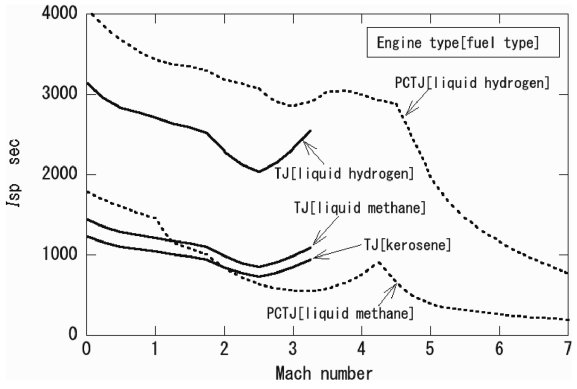

Fig. 11 Effect of fuel type on the specific impulse of a PCTJ engine with a 10-stage compressor and a TJ engine with a 5-stage compressor.

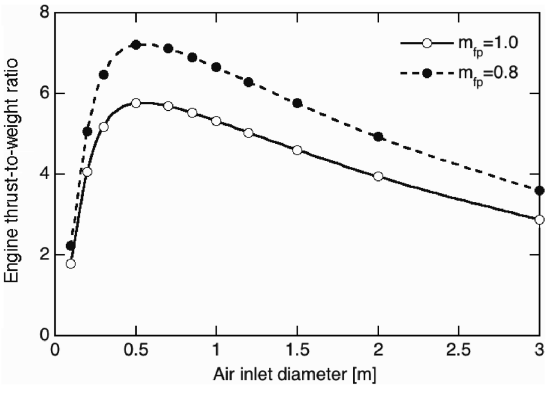

Fig. 12 Relation between thrust-to-weight ratio and diameter of air inlet of a PCTJ engine with a 10- stage compressor.

into an air-breathing engine on the bottom of the fuselage. Figure 14 shows vehicle geometry constraints must be satisfied in this problem. The fuselage height D_F must be greater than the outer diameter of the fuel tank outer diameter and the height of two engines piled up one atop the other. To satisfy these constraints, the size of the vehicle is changed, whereas the same shape and aerodynamic characteristics are maintained. The aerodynamic characteristics of the first-stage and second-stage vehicles are shown in Fig. 15. These characteristics were estimated with a tool based on the panel method described in [12].

The optimization of the ascent trajectory was from takeoff on the equator (altitude = 0 km, speed = 170 m/s) to orbit (altitude= 90 km, speed = 7937.5 m/s angle of path = 0 deg). The vehicle motion was constrained within the vertical plane, the vehicle was modeled as a point of mass, and the earth was modeled as a rotating sphere. A weight prediction method for hypersonic aerospace vehicles developed by Harloff and Berkowitz [13] was used to calculate the gross takeoff weight of the vehicle. The modifying factor for body structural weight (m_{fs}) was set as 0.8 to account for the latest material technologies because Asada et al. state that using

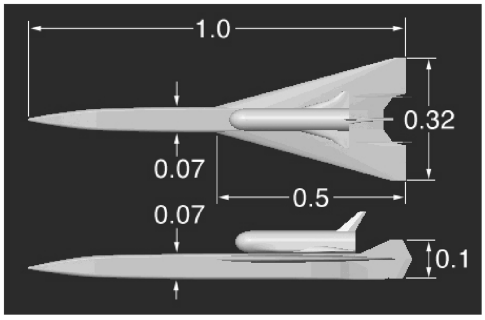

Fig. 13 Vehicle geometry.

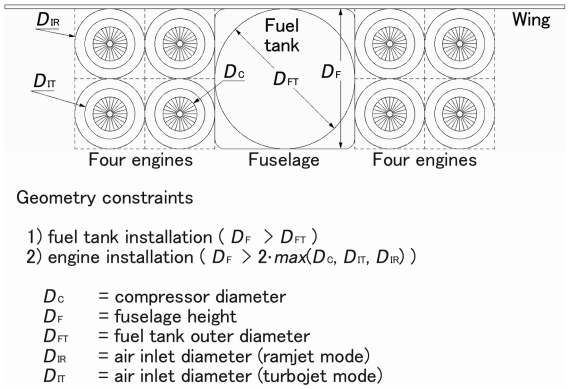

Fig. 14 Geometry constraints that the first-stage vehicle must satisfy.

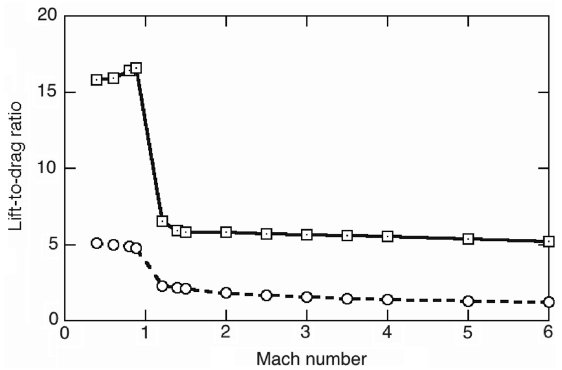

Fig. 15 Lift-to-drag ratio of the first-stage vehicle (solid line) and second-stage orbiter (dotted line).

composite materials in the main structure of the HOPE-X reduced the weight of its body structure by 20% [14].

The optimizer used in this work was a hybrid genetic algorithm (GA) with a local searching ability reinforced by using the Sequential Conjugate-Gradient Restoration Algorithm (SCGRA). Conventional optimal design methods can be classified into gradient methods and heuristic methods. Gradient methods are applicable to dynamic optimization problems (e.g., flight trajectory optimization) because of their good local search ability, but they cannot address integer variables in discrete solution spaces because it is impossible to acquire derivative information. They, therefore, cannot address all practical design processes including optimization of integer variables such as the number of air-breathing engines and the number of compressor stages. Another weak point of the gradient methods is that an unsuitable initial value easily converges to a local optimum that may or may not be equal to the global optimum. A GA, which uses heuristic methods, has no such constraint on the kind of problem because it uses no derivative information. Moreover, a GA conducts a multipoint search to obtain the global optimum solution. A disadvantage of genetic algorithms is that they can find only approximate optimal solutions. The best solution satisfying Karush–Kuhn–Tucker (KKT) optimality conditions cannot be defined using a GA. Another weak point of a GA is that its CPU cost is greater than that of an algorithm using the gradient method. Indeed, the CPU cost of a GA increases remarkably when constraints are imposed on the design space as penalty functions. The advantages of a gradient method compensate the disadvantages of a heuristic method, however, and vice versa [15]. In our hybrid GA, the SCGRA is in charge of vehicle sizing and ascent trajectory optimization with three constraints: limit dynamic pressure (50 kPa), a sufficient base area to mount all engines, and sufficient fuel in the fuel tank. The design variables optimized with the GA are listed in Table 8. A fitness function, that is, an objective function in the GA is the gross takeoff weight of the TSTO spaceplane if the required mission is accomplished. If the TSTO cannot accomplish the mission, fitness is defined as the summation of 1000 tons as the takeoff weight, of the square of the short quantity of velocity, and of the square of the short quantity of altitude. The following GA parameters were determined through trial and error to exclude initial value dependency: population in the hybrid GA = 30, number of generations = 700, and mutation rate = 0.03.

A comparative study was conducted with respect to engine type and fuel type. The 10 cases investigated are listed in Table 9. Cases 1 and 2 represent the PCTJ engines, with case 1 using liquid-hydrogen coolant and case 2 using liquid-methane coolant. Because kerosene is not a cryogenic fuel, it has little cooling effect. We, therefore, did not consider kerosene-fueled air-cooling turbojets. Cases 3, 4, and 5, respectively, represent simple hydrogen-, methane-, and kerosene-fueled turbojet engines. Because these engines have no system for thermal protection in hypersonic flight, the separation speed of the second stage must be less than Mach 3 when they are used. The effect of air precooling can be evaluated by comparing case 1 with case 3, or

Table 8 Design variables optimized with the GA

		Min.	Max.
n_c	Number of compressor stages	1	15
n_t	Number of turbine stages	1	15
n_s	Number of turbine shafts	1	3
N_e	Number of rocket engines (second stage)	1	10
ER_t	Target equivalence ratio	0.2	2.0
Reheat	Thrust augmentation by reheat	Off	On
D_F	Fuselage height, m	3.77	6.95
D_{IT}	Air inlet diameter (TJ mode), m	$0.1D_F$	$0.5D_F$
D_{IR}	Air inlet diameter (RJ mode), m	$0.1D_F$	$0.5D_F$
D_C	Compressor diameter, m	$0.2D_{IT}$	$1.0D_{IT}$
D_T	Turbine diameter, m	$0.2D_{IT}$	$1.0D_{IT}$
A_P	Heat-exchange area of air precooler[a]	100	300
V_{mc}	Mode-change speed (from TJ to RJ)	Mach 2.0	Mach 3.0
V_{sp}	Second-stage separation speed	Mach 2.0	Mach 7.0

[a]heat-exchange area divided by frontal area of compressor.

Table 9 Configurations of 10 candidates for the propulsion system of a TSTO spaceplane

Case No.	Tag	Engine type	Fuel type
1	PCTJ/H	PCTJ	Hydrogen
2	PCTJ/M	PCTJ	Methane
3	TJ/H	TJ	Hydrogen
4	TJ/M	TJ	Methane
5	TJ/K	TJ	Kerosene
6	TRJ/H-H	TRJ	Hydrogen
7	TRJ/M-M	TRJ	Methane
8	TRJ/K-H	TRJ	Kerosene (TJ mode); hydrogen (RJ mode)
9	TRJ/K-M	TRJ	Kerosene (TJ mode); methane (RJ mode)
10	TRJ/K-K	TRJ	Kerosene

case 2 with case 4. Cases 6–10 represent TRJ-engine-powered TSTO spaceplanes. We conducted a parametric study of turboramjet engines and took into account the effects of the types of fuel injected into the core-engine combustor and ram combustor. Cases 6, 7, and 10, respectively, represent hydrogen, methane, and kerosene single-fuel engines. Cases 8 and 9 represent double-fuel engines. The case 8 engine uses kerosene in the TJ mode and hydrogen in the RJ mode. The case 9 engine uses kerosene in the TJ mode and methane in the RJ mode.

B. Results

Fitness histories of the 10 cases are shown in Fig. 16, in which one sees that in all 10 cases, the design variables converged to approximately optimal values after 600 iterations of generation changes. The gross takeoff weights and mass budgets are compared in Fig. 17. The minimum gross takeoff weight (W_{gtot}) was 304 Mg and was obtained in case 6 (the vehicle powered by hydrogen-fueled TRJ engines). Side and front views of the vehicle each case are shown in Figs. 18 and 19. Optimal design variables and vehicle geometry values are summarized in Table 10.

The design variable with the greatest influence was fuel type: the gross takeoff weight can be reduced 60% by replacing kerosene fuel with liquid hydrogen due to its large heating value and cooling capacity. A smaller volume of fuel tank due to high density of kerosene or liquid methane was not an advantage because the vehicle cannot be too small for adequate engines to be installed. Because the spaceplane usually needs to have large thrust for rapid acceleration, the relative size of engine to the spaceplane is larger than that to airplanes, so reducing vehicle size by using high-density fuel is less attractive.

The multispool engine with two or three shafts was not selected except for case 5. Case 5, which is powered by a simple kerosene-fueled turbojet, has the largest gross takeoff weight because of low stage-separation speed and relatively low specific impulse. To supply enough thrust to accelerate a heavy vehicle, large numbers of compressor stages and turbine stages are needed. In other cases, a

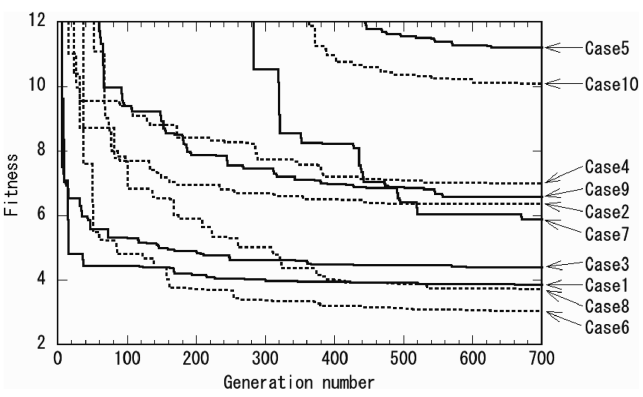

Fig. 16 Fitness history of the 10 cases.

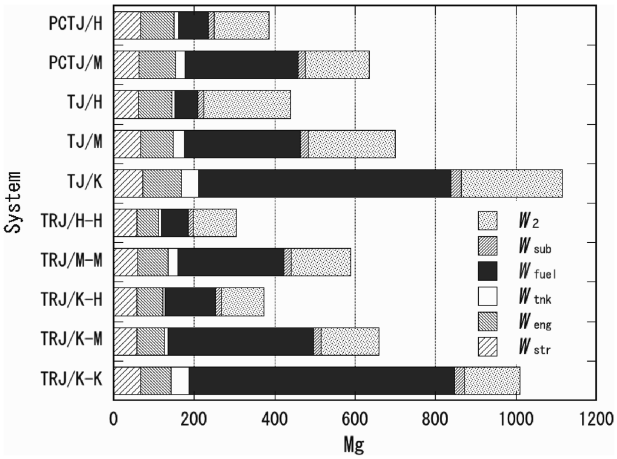

Fig. 17 Gross takeoff weights and mass budgets of the 10 cases.

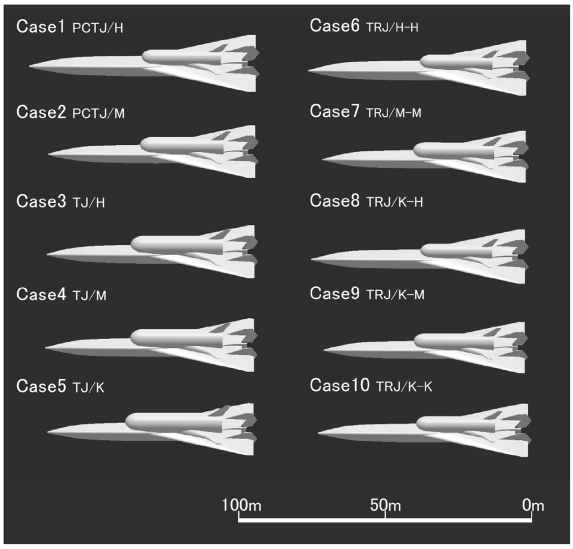

Fig. 18 Side views of the TSTO vehicles.

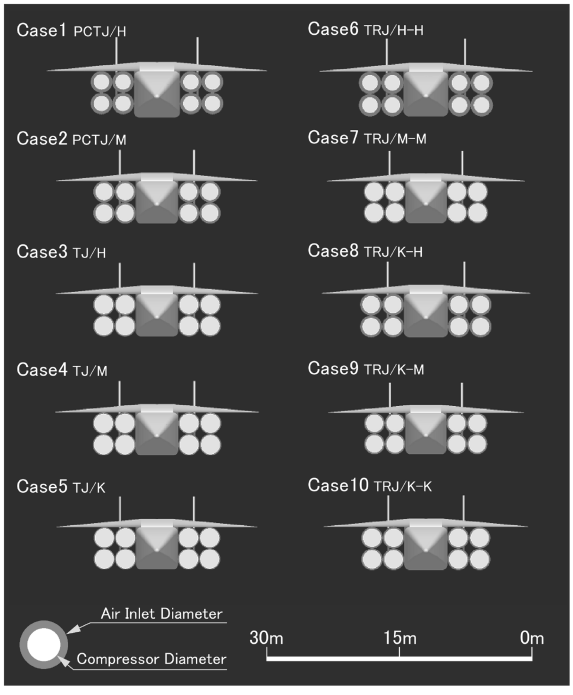

Fig. 19 Front views of the first-stage vehicles showing engine installation.

Table 10 Summary of the optimal designs

Case	1	2	3	4	5	6	7	8	9	10
Fitness rank	3rd	6th	4th	8th	10th	1st	5th	2nd	7th	9th
n_c	5	5	5	5	10	5	5	4	5	4
n_t	1	2	1	2	6	3	2	1	3	2
n_s	1	1	1	1	2	1	1	1	1	1
N_e	2	2	3	3	3	2	2	2	2	2
Reheat	On	On	On	On	On	On	On	On	On	On
ER_t	——	——	——	——	——	1.03	1.09	1.11	1.08	1.02
D_F, m	5.34	4.88	4.90	4.93	4.87	5.14	4.79	5.04	4.73	4.96
D_{IT}, m	2.48	2.44	2.45	2.46	2.44	2.01	2.39	2.29	2.22	2.40
D_{IR}, m	——	——	——	——	——	2.57	2.39	2.52	2.37	2.48
D_C, m	1.79	1.99	2.19	2.23	2.23	1.81	2.14	2.02	2.02	2.15
D_T, m	1.75	1.47	2.06	1.48	1.46	1.24	1.44	1.78	1.34	1.44
A_P,m^2	569	732	——	——	——	——	——	——	——	——
V_{mc}, Mach	——	——	——	——	——	2.21	3.00	2.17	2.23	2.44
V_{sep}, Mach	5.19	4.38	2.99	2.95	2.32	6.77	4.77	6.95	4.91	5.16
L_v, m	78.1	71.4	71.7	72.1	71.2	75.2	70.0	73.8	69.2	72.5
S_{ref}, m^2	601	502	506	511	499	557	483	536	471	517
W_{gtot}, Mg	386	636	440	700	1115	304	589	372	659	1010

single-spool four-stage or five-stage compressor was preferable. In general, engine weight reduction has priority over improved fuel efficiency for a TSTO spaceplane. The optimal speed of the second-stage separation for a TSTO spaceplane with the conventional turbojet engines without a thermal protection system (cases 3–5) is less than Mach 3, putting an excessive load on the second-stage orbiter and making the gross takeoff weight greater than that of vehicles with PCTJ or TJR engines. In these cases, as shown in Fig. 18, the size of the second stage is not well balanced with that of the first stage, and it is hard to mount the second stage on the back of the first-stage. If constraints on geometric interaction between the first- and second-stage vehicles are imposed, the rankings of case 3–5 will fall.

It can be concluded that some heat protection device for turbojet engines is indispensable if the TSTO system is to be feasible. The heat protection method best for reducing the gross takeoff weight was found to be the variable-bypass ratio used in the TRJ engine. It enables the TRJ engine to maintain a high I_{sp} at hypersonic speeds because the TRJ engine cools only the hot structure that is exposed to incoming air, whereas the PCTJ engine consumes a large amount of fuel to cool all of the incoming air. The optimal speed for switching from the TJ mode to the RJ mode was approximately Mach 2, and the optimal second-stage separation speed was Mach 7. In contrast, the optimal speed of the second-stage separation for a TSTO spaceplane with PCTJ engines (cases 1 and 2) was Mach 5, meaning that the PCTJ engine is only used at the entrance to the hypersonic region.

Comparing cases 1 and 2, we can infer that liquid hydrogen is preferable to liquid methane as a PCTJ engine coolant and fuel. In case 2, in which liquid methane is used as a coolant, the heat-exchange area needed is larger and the separation speed is lower because of the poor heat-exchange performance of liquid methane. Consequently, the gross takeoff weight in case 2 is approximately 30% greater than that in case 1 by. The MDO thus reconfirmed the advantage of using liquid hydrogen instead of liquid methane to fuel hypersonic turbojet engines.

VI. Conclusions

A comparative study of hypersonic turbojet engines was undertaken using the newly developed multidisciplinary-design-optimization environment. The hypersonic turbojet engine simulation tool used experimentally, and it statistically confirmed data to evaluate engine performance accurately. The most promising engine type for minimizing the gross takeoff weight of the TSTO spaceplane was the turboramjet engine due to its high I_{sp} at hypersonic speeds because this engine cools only the hot structure that is exposed to incoming air, whereas the precooled turbojet engine consumes a large amount of fuel to cool all of the incoming air. Liquid-hydrogen fuel was the most attractive for the hypersonic engines due to its large heating value and cooling capacity. A smaller volume of fuel tank due to high density of kerosene or liquid methane was not an advantage because the vehicle cannot be too small for adequate engines to be installed.

Acknowledgments

We thank H. Taguchi, K. Takasaki, T. Sato, T. Kojima, and T. Hirotani (Japan Aerospace Exploration Agency) for their support.

References

[1] Powell, T. H., and Glickstein, M. R., "Precooled Turbojet Engine Cycle for High Mach Number Applications," AIAA Paper 1988-2946, 1988.

[2] Sato, T., Taguchi, H., Kobayashi, H., and Kojima, T., "Development Study of Mach 6 Turbojet Engine with Air-Precooling," *Journal of the British Interplanetary Society*, Vol. 58, July/Aug. 2005, pp. 231–240.

[3] Varvill, R., and Bond, A., "The SKYLON Spaceplane," *Journal of the British Interplanetary Society*, Vol. 57, Jan./Feb. 2004, pp. 22–32.

[4] Miyagi, H., Kimura, H., Cabe, J. L., Powell, T. H., and Yanagi, R., "Combined Cycle Engine Research in Japanese HYPR Program," AIAA Paper 1998-3278, 1998.

[5] Brewer, G. D., *Hydrogen Aircraft Technology*, CRC Press, Boca Raton, FL, 1991.

[6] Tanatsugu, N., Naruo, Y., and Rokutannda, I., "Test Results on Air Turbo Ramjet for a Future Space Plane," *Acta Astronautica*, Vol. 32, No. 12, 1994, pp. 785–796. doi:10.1016/0094-5765(94)90085-X

[7] Hasegawa, H., Shimada, Y., Kashikawa, I., Yoshimura, T., Kinoshita, Y., and Kitahara, K., "Experimental Study of Compact Ram Combustor with Double-Staged Flameholders for ATR Engine," AIAA Paper 2001-3292, 2001.

[8] Sagerser, D. A., Lieblein, S., and Krebs, R. P., "Empirical Expressions for Estimating Length and Weight of Axial-Flow Components of VTOL Powerplants," NASA TM X-2406, 1971.

[9] McCarty, R. D., "Hydrogen Technology Survey-Thermophysical Properties," NASA SP 3089, 1975.

[10] Johnson, R. C., "Tables of Critical-Flow Functions and Thermodynamic Properties for Methane and Computational Procedures for Both Methane and Natural Gas," NASA SP 3074, 1972.

[11] Hatta, H., Goto, K., Sato, T., Tanatsugu, N., "Applications of Carbon-Carbon Composites to an Engine for a Future Space Vehicle," *Advanced Composite Materials*, Vol. 12, Nos. 2–3, 2003, pp. 237–259. doi:10.1163/156855103772658588

[12] Suzuki, H., and Minami, Y., "Development of Optimal Design Tool for Future Space Transportation Systems," AIAA Paper 2005-3292, 2005.

[13] Harloff, G. J., Berkowitz, B. M., "HASA-Hypersonic Aerospace Sizing Analysis for the Preliminary Design of Aerospace Vehicles," NASA CR 182226, 1988.

[14] Asada, S., Nishiwaki, K., Niitsu, M., Yamamoto, T., Kamita, T., and Kimura, G., "Development of HOPE-X All-Composite Prototype Structure," AIAA Paper 2001-1780, 2001.

[15] Kobayashi, H., and Suzuki, H., "Simultaneous Optimal Design of Hypersonic Turbojet Engine and Trajectory with SEAT," AIAA Paper 2006-8051, 2006.

O. de Weck
Associate Editor